Electromagnetically Actuated Acoustic Amplitude Modulation Synthesis

Herbert H.C. Chang
Dartmouth College
Bregman Media Labs
Hanover, NH 03755
H.Herbert.Chang.18@dartmouth.edu

Spencer Topel
Dartmouth College
Bregman Media Labs
Hanover, NH 03755
topel@dartmouth.edu

ABSTRACT

This paper discusses a new approach to acoustic amplitude modulation. Building on prior work with electromagnetic augmentation of acoustic instruments, we begin with a theory of operation model to describe the mechanical forces necessary to produce acoustic amplitude modulation synthesis. We then propose an implementation of our model as an instrumental prototype. The results illustrate that our acoustic amplitude modulation system produces controllable sideband components, and that synthesis generated from our corresponding numerical dynamic system model closely approximates the acoustic result of the physical system.

Author Keywords

acoustic synthesis, acoustic signal modulation, intermodulation, acoustic sound module, augmented instrument, electromagnetism, harmonic oscillators

ACM Classification

H.5.5 [Information Interfaces and Presentation] Sound and Music Computing, H.5.2 [Information Interfaces and Presentation] User Interfaces—Haptic I/O, I.2.9 [Artificial Intelligence] Robotics—Propelling mechanisms.

1. INTRODUCTION

Recent expansion of electromagnetically (EM) augmented instruments illustrates a growing interest in acoustic synthesis. These approaches access new properties of an acoustic instrument through EM excitation, and are capable of generating sonic results strongly resembling electronic sound synthesis.

A particularly challenging aspect of augmented EM instrument design is the description and evaluation of underlying system dynamics. Many augmented acoustic instruments demonstrate complex sonic behaviors without modifications [6, 10]. Complexity arises from interactions between acoustic instruments and EM augmentations. Nonlinearities within these systems, including signal modulation, are even more difficult to account for and still more challenging to control [19, 20].

Our investigation focuses on acoustic amplitude modulation (AAM) of driven harmonic oscillators. The aim is to use a dynamic model approach to AAM and present an EM augmented harmonic oscillator capable of producing acoustic amplitude modulation.

2. PRIOR WORK

We adopt the definition of acoustic synthesis as a "sound-generating process in which synthesis is carried out in acoustical terms: frequency, spectrum, waveform, amplitude, modulation, and so on." [5]. Early systems exhibiting acoustic synthesis include the Helmholtz synthesizer [18], and later the Rhodes Piano "tone-bar" system [21]. Recent EM Augmented instruments include actuation of strings [2, 3, 8, 14, 17], metal bars, asymmetric tuning forks [4, 24], and non-pitched percussion [19, 20]. In these instruments, EM actuation is presented as an alternative to conventional actuation, providing means to shape or sustain sound in new ways [17].

2.1 Acoustic Signal Modulation

Two notable historical precedents exist in acoustic signal modulation synthesis. Both systems were developed for the electronic organ: the Hammond *Tone Cabinet* and the Leslie speaker, shown in Figure 1.

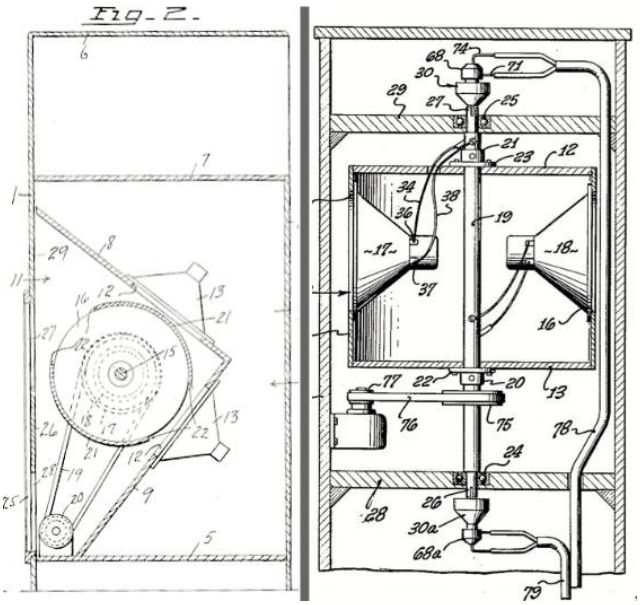

Figure 1: Patent images for the *rotor tremulant* used in the Hammond Organ (left), and the "mercury slip-ring assembly" used in the Leslie Speaker Cabinet (right). [7, 12]

NIME'16, July 11-15, 2016, Griffith University, Brisbane, Australia.

The Hammond design produces AAM synthesis, whereas the Leslie design produces Acoustic Frequency Modulation (AFM) synthesis by exploiting the Doppler effect through rotation of directional sound sources [9]. The Hammond Organ Company implemented a *rotor tremulant* invented by B. Hartsough to produce a tremolo-like effect using acoustic amplitude modulation [7]. Hammond modified an existing tone cabinet, the D-20, to include a rotor drum in the DXR-20 and XR-20 tone cabinets [26]. The Hammond rotor drum generates acoustic AM using a spinning drum with slotted vents that filter sound generated from small speakers. The Hammond and Leslie systems are limited by rotational rate and sound propagation, thus limiting the frequency range to exclusively narrow-band (tremolo-like) modulation.

We encountered similar limitations in earlier prototypes utilizing a rotating aperture and tuning fork design, due to the high RPM's required to produce higher frequency sideband components. In an effort to overcome this problem, we offer a Time-Varying Damping (TVD) solution presented first as a theory-of-operation in Section 3 and then as an instrumental prototype in Section 4.

3. AAM THEORY OF OPERATION

3.1 Signal Modulation

Signal modulation is the process of combining two signals into a third signal containing desired properties of both signals, such as frequency sideband. In the time-domain this corresponds to multiplication of carrier and modulator signals with the mathematical form,

$$A(t) = M(t) \times C(t) = M(t) \times C_0 \cos(\omega_c t) \tag{1}$$

where $A(t)$ is the resultant signal, $M(t)$ is the modulator signal, and $C(t)$ is the carrier signal with constant frequency ω_c. Equation 1 applies for all forms of Amplitude Modulation (AM), including Acoustic Amplitude Modulation (AAM). To illustrate sideband generation, we assume constant frequency for a time-varying modulator envelope function $M(t) = \cos(\omega_r t)$. Then A(t) is of the form:

$$\begin{aligned} A(t) &= cos(\omega_r t) \times C_0 \cos(\omega_c t + \delta) \\ &= \frac{1}{2} C_0 [\cos((\omega_c + \omega_r)t + \delta) - \cos((\omega_c - \omega_r)t - \delta)] \end{aligned} \tag{2}$$

with δ the phase angle. $A(t)$ includes the desired sideband components in the set $\omega AM = \{\omega_c \pm \omega_r\}$ in $\cos(\omega_c + \omega_r)$ and $\cos(\omega_c - \omega_r)$ shown in equation 2. This amplitude modulation through the nonliniearities of two or more frequencies is known as intermodulation.

Harmonic sidebands of the form $\omega AM = \{\omega_c \pm n \cdot \omega_r | n \in \mathbb{N}\}$ occur when the carrier signal is overdriven. Intermodulated sidebands occur as a linear combination of the carrier and the modulating signal, which produce a continuous range of sidebands that can intersect harmonic sidebands. Additionally, the frequency of the modulator need not be constant and any $M(t)$ can be used to modulate a carrier using the Fourier Transform. AAM synthesis of sidebands components arise by the same principle in a physical system.

3.2 Dynamic System Model

We describe AAM as a dynamic system under a Single Degree of Freedom (SDOF), illustrated in Figure 2. The system consists of an acoustic carrier harmonic oscillator and a modulator-actuated TVD mechanism, where m and k are mass and spring constants, respectively. The oscillator is driven by $F(t)$. The system is described by the equations of motion (EOM) in sections 3.3 and 3.3.2.

System inputs for the carrier and modulator signals are defined as two generic oscillators or unit generators, where $\bigotimes_{car}$ corresponds to the carrier signal and $\bigotimes_{mod}$ corresponds to the modulator signal. These signals are then transformed into electromagnetic force as described in [15].

3.3 SDOF Equations of Motion

If an object's position is directly related to acoustic amplitude, then we can model acoustic amplitude as a function of position with a SDOF. This section develops the theory of tracking the position of mass m.

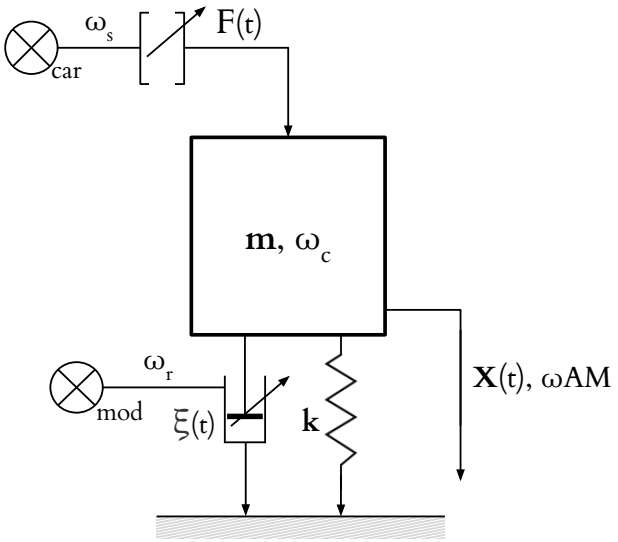

Figure 2: Free body diagram of the AAM dynamic model of.

3.3.1 Driven Harmonic Oscillator

When the object's natural frequency is actuated, it is in resonance. The natural frequency ω_c of a harmonic oscillator is dependent on mass m and spring constant k, given by the relationship $k = \omega^2 m$. Its position $X(t)$ satisfies the following differential equations:

$$mx''(t) + \xi x'(t) + kx(t) = F(t) \tag{3}$$

$$x''(t) + \frac{\xi}{m} x'(t) + \omega^2 x(t) = \frac{F(t)}{m} \tag{4}$$

where m is the mass of the object and ξ is the material's damping coefficient. The carrier signal is generated by actuating the system's consistent natural frequency, using input signal ω_s. This produces the driving force denoted in Equation 5. Under EM actuation, an input's signal frequency is typically one half ($n = 2$) or one fourth ($n = 4$) the carrier frequency [15].

$$F(t) = F_0(\cos(n\omega_s t) + 1) = F_0(\cos(\omega_c t) + 1) \tag{5}$$

When one strikes a tuning fork, its sound gradually decreases in volume. This corresponds to the transient dissipation of energy after an initial force, described by x_1 and x_2 in equation 6. The coefficients of x_1 and x_2 are zero if the mass is initially at rest. With constant and positive m, ξ and k, with the mass initially at rest, the motion of mass m is govern by the steady state solution in Equation 7:

$$X(t) = c_1 x_1(t) + c_2 x_2(t) + A\cos(\omega_c t) + B\sin(\omega_c t) \tag{6}$$

$$X(t) = A\cos(\omega_c t) + B\sin(\omega_c t) = M_0 \cos(\omega_c t + \delta) \tag{7}$$

where A and B depend on F_0 and are then reformulated as M_0 and the phase angle δ.

When the driving frequency ω is equal to the carrier frequency ω_c, the coefficient M_0 is given as:

$$M_0 = \frac{F_0}{\sqrt{m^2(\omega_c - \omega)^2 + \xi^2\omega^2}} = \frac{F_0}{\xi\omega_c} \tag{8}$$

where $\omega_c - \omega = 0$. This expression is only correct when m, ξ, and k are constants, yet the inverse relation in equation 8 suggests amplitude M_0 can be modulated by varying either the driving frequency $F(t)$ or damping value ξ.

3.3.2 *Modulation via TVD*

The driving frequency must be held constant to produce a consistent carrier signal, thus we produce Acoustic Amplitude Modulation using Time-Varying Damping (TVD), using a similar approach found in variable impedance actuators and variable dampers utilized in anti-oscillatory systems such as robotics, active vehicle suspensions, and earthquake mitigation systems [27, 16, 11]. This is best achieved if certain conditions are met:

1. The object is driven at its resonance frequency i.e. $m^2(\omega_0 - \omega)^2 = 0$
2. Change damping value ξ is small enough so that the natural frequency is the same, yet big enough to change the amplitude of ω_c.

ξ is now a function of time, where $X(t)$ satisfies the following differential equation:

$$x''(t) + \frac{\xi(t)}{m}x'(t) + \omega^2 x(t) = \frac{F(t)}{m} \tag{9}$$

The position of a mass under TVD can only be solved numerically, but we can illustrate periodic damping modulation based on the relationship in Equation 8. We choose $\xi(t)$ such that $M(t)$ is unipolar and sinusoidal and then combine it with Equation 7.

$$\begin{aligned} M(t) &= \frac{F_0}{\xi(t)\omega_c} = \frac{F_0}{\xi_0\omega_c}(\cos(\omega_r t) + 1) \\ X(t) &= M(t)\cos(\omega_c t + \delta) \\ &= (\frac{F_0}{\xi_0\omega_c} + 1)\cos(\omega_r t) \times \cos(\omega_c t + \delta) \\ &= C_0[\cos((\omega_c + \omega_r)t + \delta) - \cos((\omega_c - \omega_r)t - \delta)] \end{aligned} \tag{10}$$

where C_0 is the combined constant coefficient. If the modulating signal is periodic, the measured sidebands are $\omega_{AM} = \omega_c \pm \omega_r$. This formulation of intermodulation produces sidebands consistent with Equation 2. We later solve for $X(t)$ numerically with $\xi = \cos(\omega_r t)$ and compare the synthesis model to the acoustic synthesis of the AAM Prototype in Section 5.2.

4. AAM PROTOTYPE

4.1 Design

Figure 3 illustrates the basic configuration of the AAM prototype design. This design contains all the functional elements of the dynamic system model presented in Section 3.2 consisting of the following active components:

1. **Acoustic Carrier Harmonic Oscillator** A driven harmonic oscillator composed of an EM actuator and a tuning fork.
2. **Modulator-Actuated TVD**: An actuated TVD mechanism, consisting of an EM actuator and an acoustic damping surface or medium.
3. **Stabilization Mechanism**: spring-loaded stabilization frame restores the tuning fork to the zero position.

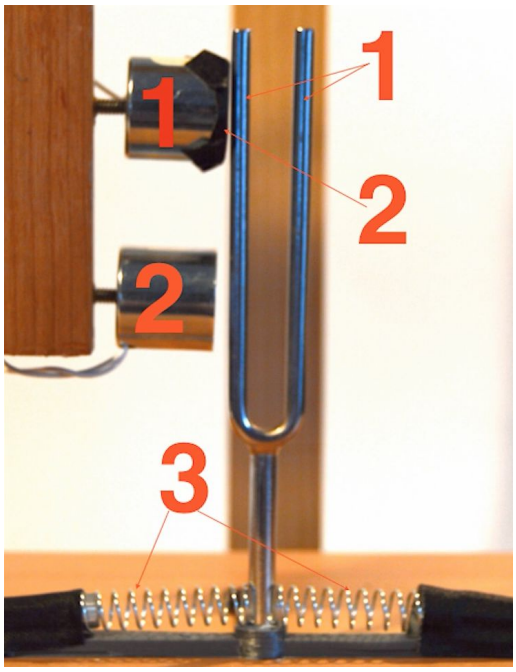

Figure 3: AAM prototype layout with three active components 1. Acoustic Carrier Harmonic Oscillator, 2. Modulator-Actuated TVD, 3. Stabilization Mechanism

4.1.1 *Acoustic Carrier Harmonic Oscillator*

A harmonic oscillator consisting of a tuning fork produces the acoustic carrier signal in the AAM prototype. The symmetric tine movement of the fork generates an efficient, almost perfectly sinusoidal motion in the stem. Since, their motions are coupled, modeling the position of the tines directly describes the motion of the stem and its acoustic effect [23]. A cylindrical EM actuator drives the tines of a steel tuning fork at half or one-fourth its natural frequency, since both positive and negative magnetic flux attracts ferromagnetic objects [15]. This configuration produces two salient carrier signals, the natural frequency ω_{c1} and twice its natural frequency ω_{c2}.

4.1.2 *Modulator-Actuated TVD*

Displacement of the fork tines determines the amplitude of the periodic output signal, thus modulating the displacement of the forks through damping produces amplitude modulation. The second EM actuator applies force to the fixed stem and causes it to pivot slightly. Since the angle is small and contact area is small, TVD is linearlized and modeled as horizontal displacement of the tines in Figure 3. Contact between the tuning fork tine and damping material on the carrier AM actuator produces the modulator-actuated TVD effect. This corresponds to a nonsinusoidal, periodic modulation signal. Since the constant signadrivel frequency from the carrier electromagnet continues to excite the tines, the natural frequency of the tuning fork appears to remain the same. This is likely because damping only occurs to a limited cross section of the tine, while the rest of the tuning fork is unaltered.

4.1.3 Stabilization Mechanism

A third component is a suspension system consisting of a three-leg base with a hole for a tuning fork and two compression springs. Two end-blocks control the tension of the springs to accommodate different diameter harmonic resonators. This construction provides restoring-force to return to the mass's equilibrium position.

4.1.4 Isolation and Amplification

Additional non-active components decouple the force generating noise from the desired AAM signals and acoustically amplify the signals. Using a T-Frame design we separate the structure holding the electromagnets from the tuning fork and stabilization mechanism. This decreases signal bleed caused by vibration and other noise generated by the EM actuators. Sound isolation pads further reduce propagation of noise through a table or stand. To amplify the desired signals, we employ a thin soundboard acoustic resonator consistent with surfaces commonly used to amplify tuning forks.

4.2 Implementation

Our implementation of the AAM prototype, pictured in Figure 4, implements the three active design elements listed in Section 4.1. The components described below are the same as those evaluated in Section 5.2. The physical components and specifications are as follows:

- Tuning fork with a natural frequency of ($\omega_c = 419.41$ Hz), driven at half it's natural frequency ($\omega_s = 209.7$ Hz).
- EM actuators (two) E-77-82 [13].
- Damping material consisting of a 0.27mm thick coated-cloth with a synthetic rubber adhesive. In resting position, there was a small gap of approximately 2mm between the tine of the fork and the surface of the damping material.
- Spring suspension system consisting of three-leg base made from 3D printed ABS plastic, two small steel compression springs with the with a length of 35mm and a diameter of 9mm tension springs, and adjustable steel end-blocks.
- Sound board made from cedar wood, with the dimensions 381 mm, 254 mm, 12 mm (L,W,H), resting on laterally configured hardwood stands with the dimensions 152 mm, 25 mm, 25 mm (L,W,H).
- Hardwood frame supporting and isolating the EM actuators, and acoustic isolation pads (not pictured) lifting separately the soundboard and the hardwood frame.
- SMSL SA-50 Class D 50 Watt amplifier for the EM actuators with signals generated on a MacBook pro running max 7.

5. EVALUATION AND RESULTS

5.1 Method

To compare the dynamic system model and the AAM prototype, we developed three tests involving manipulation of the modulating frequency ω_r The first test consisted of five non-continuous modulations at fixed modulator increments of approximately 83 Hz, between 5 Hz and 420 Hz, each lasting 7 s, with 2 s silence in between. The second test consists of a 40 s linear envelope function sweep from 0 Hz to 210 Hz and back to 0 Hz. We also wanted evaluate for overmodulation in the AAM prototype, so we created a third test where $\omega_r > \omega_c$. This was accomplished through increasing amplification of the modulator ω_r, resulting in additional harmonic sidebands [22]. Our rationale for developing these comparisons was to confirm our model describes the audible sideband component behavior in common applications for AM in music audio synthesis. The results of these tests are presented in 5.2.

Figure 4: AAM Prototype: This is implementation consists of a harmonic oscillator and acoustic amplitude modulation with parametric control of sideband components.

5.1.1 Synthesis Evaluation Method

To evaluate the AAM prototype and the dynamic model together, we constructed a numerical model in Matlab to synthesize audio using equations from Section 3. These simulations were then synthesized and analyzed in Section 5.2, at a sampling rate of 44100 Hz at 16 bit resolution.

5.1.2 Acoustic Evaluation Method

The AAM prototype was tested in a -60dB environment, with an Earthworks QTC50 omnidirectional microphone at a distance from the soundboard of 20mm. The audio was recorded in Ableton Live 9 using a Focusrite RedNet audio interface with a True Precision pre-amp, at a sampling rate of 44100 Hz at 16 bit resolution. The AAM prototype setup was identical to the specifications described in Section 4.2.

Analysis was conducted using the open-source Baudline time-frequency analyzer. We generated spectrograms using the Fourier transform with a transform size of 32768, and a Hanning window, with a hop-size of 256 using optimal (100%) Drift Integration [25].

5.2 Results

Figure 5 shows the spectrograms for the three tests described in Section 5. The model simulated the production of primary harmonic sidebands in the modulated condition. The third column in Figure 5 shows the results for the overmodulation conditions. This resulted in prominent second and third sideband harmonics, and inconsistent higher harmonics.

Additional components, including a low-frequency sweep in the sweep test from 0 Hz to 105 Hz to 0 Hz, and a 205 Hz component in both tests are primarily attributable to signal-bleed from the ω_r and ω_s. A third component at approx. 105 Hz appears in both the modulated and overmodulated AAM prototype spectrograms, and is subharmonic generated from vertical oscillation of the tuning fork against the soundboard [23]. It is interesting to also note the perturbations along the linear striations in both tests. We posit these resonances are likely resulting from nonlinearities in

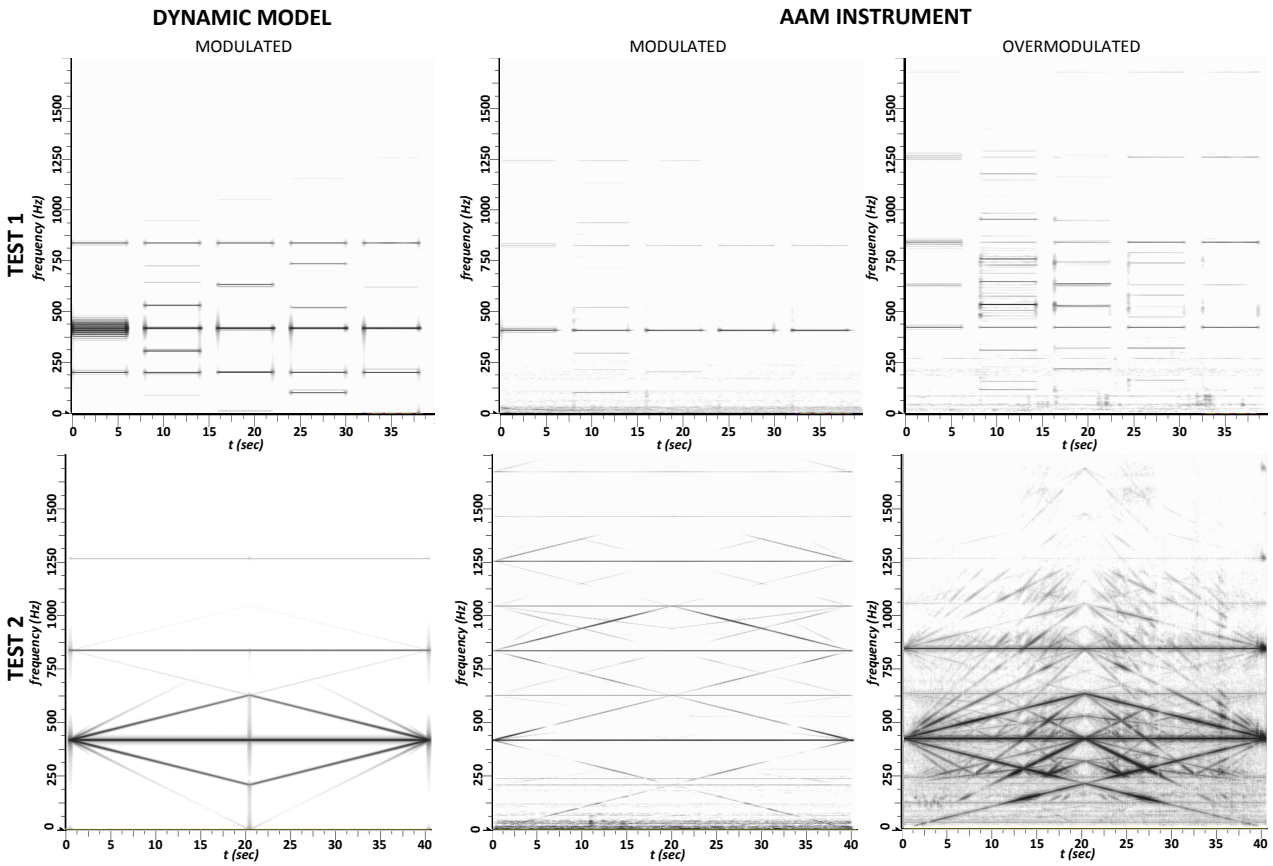

Figure 5: Spectrogram evaluations of the Dynamic Model and the AAM prototype. Non-continuous step modulation test (top row), continuous-sweep test (bottom row)

the physical system, specifically from the non-sinusoidal periodic motion in the TVD implementation.

Results for the non-continuous step modulation test in the top row of Figure 5, show certain sidebands appearing more clearly with certain modulator frequencies. For instance, the first three steps AAM prototype are clearly accounted for in the dynamic model synthesis, whereas the last two steps are nearly indiscernible in the modulated condition and only weakly visible in the overmodulated condition. This is likely a result of efficiency problems in the EM actuator discussed further in Section 5.3.

Specific to the continuous-sweep test, there are intersections of the sidebands of ω_{c1} and ω_{c2}, which generate greater sound intensity. These are shown as noticeable vertical striations in the modulated and overmodulated iterations of the test, shown as both dark and bright streaks in the AAM prototype spectrograms. These areas denote nodes and antinodes, where the modulation frequency and its multiples form relatively simple integer ratios of the carrier frequency.

Comparing the dynamic model and the AAM prototype further shows that the loudest sidebands at 105 Hz are considerably more prominent in the AAM prototype, while the model produces strong sidebands at twice the modulating frequency [15]. The *Klang* mode, roughly 6.25 times the natural frequency, of the tuning fork is also present in the AAM prototype evaluation.

5.3 Additional Observations

5.3.1 Improving Implementation of TVD

Additional experimentation found that the EM actuator in the TVD system is inefficient at generating displacement or movement of mass m at frequencies above 80 Hz, with a decreasing efficiency toward an upper limit of approx. 350 Hz. This is consistent with prior observations of EM transduction [15].

Given this limitation, it is worth noting that an EM modulated TVD system still produces AAM at significantly higher modulation frequencies than previous acoustic signal modulation systems discussed in Section 2. Therefore, development of a more suitable implementation of TVD system offers the best opportunity for increasing modulation frequency range and improving overall efficiency. This would also allow analysis on the specific weight of sidebands between the numerical and physical model.

Another limitation of this prototype is the relatively quiet production of the acoustic signal, which in turn adversely effects the Signal-to-Noise Ratio (SNR). Improvements might include the use of different acoustic amplification, such as horns or more efficient soundboards, or through the application of acoustic or transducer electric amplification.

6. CONCLUSION AND FUTURE WORK

6.1 AAM Prototype Extensions

Materiality is a notable feature of acoustic synthesis systems and EM augmented instruments [5, 14]. We consider here features that we plan to investigate in future work:

- **Live Input**: Substitution of the oscillator driven modulator with a signal-corrected live input.
- **Feedback and DSP**: Create self-feedback using a pickup or via acoustic feedback, or using sonic transducers to modify the signal through subtractive or additive synthesis.

- **Multi-Degree of Freedom Systems**: Generating complex timbres using a set of harmonic oscillators amplified on the same resonator or network of resonators.
- **Material Variation**: Utilization of different soundboards, dampers, harmonic resonators, and actuators.
- **Scaled Implementations**: Develop a set of physical effects at a different scale that can operate inside electronic systems [1].

6.2 Conclusion

In this paper we introduce a new approach to Acoustic Amplitude Modulation. Starting from prior work in acoustic signal modulation and EM augmented instruments, we develop a dynamic model to explain the underlying mechanics of AAM. A prototype AAM instrument is implemented in the form of a driven harmonic oscillator with controllable time-varying damping modulation. Sonic results show that consistent acoustic sideband components can be produced and manipulated in an acoustic system utilizing a driven harmonic oscillator [1].

Our results also show that a dynamic model describes the primary sideband harmonics generated by the physical system. AAM and more broadly, acoustic signal modulation, point to a new direction in EM augmented instrument research. It is one that offers rich sonic possibilities for instruments and effects, and nearly limitless variation through materials, processing, and configuration.

7. ACKNOWLEDGMENTS

We would like to thank Michael A. Casey and Paula Matthusen for their helpful feedback. This work was partially supported by the Office of Undergraduate Research at Dartmouth College.

8. REFERENCES

[1] 1010.co.uk. Erd modular eurorack series 2015. `http://www.1010.co.uk/org/ERD.html`, 2015. Accessed: 2016-01-23.

[2] E. Berdahl, S. Backer, and J. Smith. If i had a hammer: Design and theory of an electromagnetically-prepared piano. In *Proc.of ICMC*, pages 81–84, 2005.

[3] E. Berdahl, G. Niemeyer, and J. O. Smith. Active control of a vibrating string. *The Journal of the Acoustical Society of America*, 123(5):3666–3666, 2008.

[4] N. C. Britt, J. Snyder, and A. McPherson. The emvibe: an electromagnetically actuated vibraphone. In *Proc. New Interfaces for Musical Expression*, 2012.

[5] C. Cadoz, A. Luciani, J.-l. Florens, C. Roads, and F. Chadabe. Responsive input devices and sound synthesis by stimulation of instrumental mechanisms: The cordis system. *Computer music journal*, pages 60–73, 1984.

[6] C. Camier, C. Touzé, and O. Thomas. Non-linear vibrations of imperfect free-edge circular plates and shells. *European Journal of Mechanics-A/Solids*, 28(3):500–515, 2009.

[7] B. Hartsough. Tone cabinet for electric organs, Sept. 28 1948. US Patent 2,450,139.

[8] G. S. Heet. String instrument vibration initiator and sustainer, Feb. 28 1978. US Patent 4,075,921.

[9] C. A. Henricksen. Unearthing the mysteries of the leslie cabinet. *Recording Engineer/Producer magazine, April*, 1981.

[10] M. Keane. Understanding the complex nature of piano tones. *Acoustics Research Centre. Available from http://www.acoustics.auckland.ac.nz/research/research_files /keane _nzas04.pdf*, 2004.

[11] U. Kurata, T. Kobori, M. Takahashi, N. Niwa, and H. Midorikawa. Actual seismic response control building with semi-active damper system. *Earthquake Eng. Struct. Dyn*, 28:1427–1447, 1999.

[12] D. Leslie. Mercury slip ring assembly, Dec. 19 1961. US Patent 3,014,192.

[13] Magneticsensorsystems.com. Tubular electromagnet. `http://www.magneticsensorsystems.com/electromagnet/tubular/E-77-82.asp`, 2016. Accessed: 2015-01-11.

[14] A. McPherson. The magnetic resonator piano: Electronic augmentation of an acoustic grand piano. *Journal of New Music Research*, 39(3):189–202, 2010.

[15] A. McPherson. Techniques and circuits for electromagnetic instrument actuation. In *Proceedings of the Twelfth International Conference on New Interfaces for Musical Expression*, 2012.

[16] B. V. Murty. Electric, variable damping vehicle suspension, Mar. 28 1989. US Patent 4,815,575.

[17] D. Overholt, E. Berdahl, and R. Hamilton. Advancements in actuated musical instruments. *Organised Sound*, 16(02):154–165, 2011.

[18] D. Pantalony. Seeing a voice: Rudolph koenig's instruments for studying vowel sounds. *The American journal of psychology*, pages 425–442, 2004.

[19] A. Piepenbrink and M. Wright. The bistable resonator cymbal: An actuated acoustic instrument displaying physical audio effects. 2015.

[20] D. Rector and S. Topel. Emdrum: An electromagnetically actuated drum. In *Proceedings of the Fourteenth International Conference on New Interfaces for Musical Expression*, 2014.

[21] H. Rhodes. Piano dampening mechanism, Dec. 14 1948. US Patent 2,456,321.

[22] C. Roads. A tutorial on non-linear distortion or waveshaping synthesis. *Computer Music Journal*, pages 29–34, 1979.

[23] T. D. Rossing, D. A. Russell, and D. E. Brown. On the acoustics of tuning forks. *Am. J. Phys*, 60(7):620–626, 1992.

[24] G. Shear. *The electromagnetically sustained Rhodes piano*. PhD thesis, Univ. of Santa Barbara, 2011.

[25] T. Thompson. Baudline signal analyzer - fft spectrogram. `http://http://www.baudline.com/`, 2010. Accessed: 2016-01-20.

[26] T. Thompson. Mosweb online! tone cabinet database. `http://mosweb.federalproductions.com/knowledgebase/tone-cabinet-database/`, 2011. Accessed: 2016-01-01.

[27] B. Vanderborght, A. Albu-Schäffer, A. Bicchi, E. Burdet, D. G. Caldwell, R. Carloni, M. Catalano, O. Eiberger, W. Friedl, G. Ganesh, et al. Variable impedance actuators: A review. *Robotics and Autonomous Systems*, 61(12):1601–1614, 2013.

[1]For a video summary of this paper, please visit: `https://vimeo.com/153815744`. Additional media, and designs available at: `https://goo.gl/ssbrSs`